DOI:
Article type: Full Paper

Amphiphilic Core-Shell Nanocomposite Particles for Enhanced Magnetic Resonance Imaging

Lianghui Chen, Dechao Niu, Cheng Hao Lee, Yuan Yao, Ki Lui, Kin Man Ho, Pei Li**

L. Chen, Dr. D. Niu, Dr. C. H. Lee, Y. Yao, Dr. K. Lui, Dr. K. M. Ho, Prof. P. Li
Department of Applied Biology and Chemical Technology
The Hong Kong Polytechnic University
Hong Kong, China
Email: pei.li@polyu.edu.hk

Dr. D. Niu
Lab of Low-Dimensional Materials Chemistry
School of Materials Science and Engineering
East China University of Science and Technology
Shanghai 200237, China
Email: dcniu@ecust.edu.cn

Dr. Ki Lui
Division of Science & Technology
The Hong Kong Community College
Polytechnic University of Hong Kong
Hong Kong, China

Keywords: core-shell nanocomposite; magnetic nanoparticle; MRI contrast agent; T_2 relaxivity

Abstract: We have designed and developed a scalable synthesis of magnetic core-shell nanocomposite particles as a novel class of magnetic resonance (MR) contrast agent. Each nanocomposite particle consists of a biocompatible chitosan shell and a poly(methyl methacrylate) (PMMA) core where multiple aggregated γ-Fe_2O_3 nanoparticles are confined within the hydrophobic core. Properties of the nanocomposite particles including their chemical structure, particle size, size distribution, and morphology, as well as crystallinity of the magnetic nanoparticles and magnetic properties were systematically characterized. We have evaluated their potential application as an MR contrast agent. Results showed that the nanocomposite particles had good stability in biological media and very low cytotoxicity in both L929 mouse fibroblasts (normal cells) and HeLa cells (cervical cancer cells). They also exhibited excellent MR imaging performance with a T_2 relaxivity of up to 364 $mM_{Fe}^{-1}\ s^{-1}$. An *in vivo* MR test performed on a naked mouse bearing breast tumor indicated that the nanocomposite particles could localize in both normal liver and tumor tissues. These results suggest that the magnetic core-shell nanocomposite particles are an efficient, inexpensive, and safe T_2-weighted MR contrast agent for both liver and tumor MR imaging in cancer therapy.

1. Introduction

Magnetic resonance imaging (MRI) is based on detecting nuclear magnetic resonance (NMR) signals emitted by hydrogen protons in the body under a magnetic field. Nowadays, this imaging modality is widely used around the world to diagnose and monitor human diseases because it is non-invasive, safe, and gives high spatial resolution images.[1] Many MRI examinations use contrast agents to increase sensitivity and enhance the quality of images for a more accurate diagnosis.[2] The MRI contrast agents can be categorized into two broad groups: T_1 and T_2 agents. Iron oxide-based nanoparticles, commonly used as T_2 agents and negative contrast agents, have attracted increasing research interest owing to several of their advantages such as high negative T_2 contrast effect (r_2 relaxivity), size-tunability, and low cytotoxicity *in vivo* application.[3] The high negative contrast effect stems from the acceleration of the transverse relaxation process of water protons in the vicinity of local magnetic perturbations induced by iron oxide nanoparticles with a strong magnetic moment.[2] Based on this outer-sphere relaxation theory, a variety of iron oxide-based MR contrast agents with high r_2 relaxivity have been designed and prepared through fine-tuning their particle size,[4] shape,[5] chemical composition,[6] and surface modifications.[7-9] For example, Bao *et al*. have reported that the r_2 relaxivity of iron oxide nanoparticles (~14 nm in diameter) can reach 385 $mM_{Fe}^{-1}s^{-1}$ when coated with 1,000 Da polyethylene glycol (PEG).[10] Recently, new strategies to increase r_2 relaxivity through confinement and aggregation of ultra-small superparamagnetic iron oxide (USPIO) with a diameter less than 50 nm have been developed. Cheon and Shin *et al*. have reported that confining several iron oxide nanoparticles on the surface of silica particles could enhance the r_2 relaxivity to up to 397 $mM_{Fe}^{-1}s^{-1}$.[11] Shi *et al*. have also developed an efficient approach to encapsulate multiple magnetite nanoparticles into the silica cross-linked block copolymer micelles, thus enhancing the r_2 relaxivity to up to 379.6 $mM_{Fe}^{-1}s^{-}$.[12]

Although these methods to synthesize iron oxide-based MR contrast agents could give high r_2 relaxivity, they involve time-consuming and complicated synthetic procedures as well as the use of expensive reagents, thus limiting their scalability. Therefore, the developing of simple and scalable methods to synthesize iron oxide-based MR contrast agents with high r_2 relaxivity and specificity, low toxicity, high contrast enhancement with low dosage *in vivo*, and with minimal costs is still a great challenge.

Herein we describe our design and synthesis of a new class of iron oxide-based amphiphilic nanocomposite particles as potential MR contrast agents. The nanocomposite particles consist of biocompatible chitosan shells and poly(methyl methacrylate) (PMMA) cores with multiple γ-Fe_2O_3 nanoparticles aggregated and confined in the hydrophobic cores. These nanocomposite particles possess several advantageous features: 1) The hydrophobic PMMA core can embed multiple γ-Fe_2O_3 nanoparticles and confine the aggregation within the nano-sized core. 2) The hydrophobic core can prevent leakage and acid attack of the magnetic nanoparticles, as well as avoid interaction between biomolecules and iron oxide nanoparticles. 3) The hydrophilic chitosan shell provides surface functionality and colloidal stability in an aqueous environment. 4) The magnetic core-shell nanocomposite particles are biocompatible with low cytotoxicity. 5) Synthesis of the nanocomposite particles is based on emulsion polymerization, which is feasible for scale-up production. Finally, we have evaluated the magnetic core-shell nanocomposite particles through studies of their *in vitro* and *in vivo* MR properties.

2. Results and Discussion

2.1 Synthesis of magnetic core-shell nanocomposite particles

Scheme 1 shows the synthesis of nanocomposite particles made up of chitosan shells and PMMA cores that contain multiple aggregated γ-Fe_2O_3 nanoparticles (γ-Fe_2O_3@PMMA/CTS). This synthetic route is based on our previously established methods but improved with the use of a greener hydrogen peroxide instead of *t*-butyl hydroperoxide as the redox initiator.[13, 14] The synthesis of γ-Fe_2O_3@PMMA/CTS particles involved a two-stage reaction: 1) Preparation of vinyl-coated γ-Fe_2O_3 nanoparticles through surface modification of citrate-coated γ-Fe_2O_3 nanoparticles with tetraethylorthosilicate (TEOS), followed by reaction with 3-(trimethoxysilyl)propyl methacrylate (MPS). 2) Preparation of magnetic core-shell nanocomposite particles via the hydrogen peroxide-induced graft copolymerization of methyl methacrylate (MMA) from chitosan in the presence of vinyl-coated γ-Fe_2O_3 nanoparticles, followed by emulsion polymerization. The γ-Fe_2O_3@PMMA/CTS nanocomposite particles were isolated by removing those particles that were without or that contained an insufficient quantity of magnetic nanoparticles using a magnetic column with a magnetic field gradient (4 Tesla).[15] Encapsulation efficiency of the polymerization to produce γ-Fe_2O_3@PMMA/CTS nanocomposite particles was gravimetrically determined and the results are shown in **Table 1.**

Scheme 1

Since several studies have suggested that transverse relaxivity could be enhanced through the aggregation of magnetic nanoparticles,[16, 17] we attempted to increase the aggregation degree of iron oxide nanoparticles within the core region by increasing the dosage of vinyl-coated γ-Fe_2O_3 nanoparticles (Supporting information, Table S1 shows detailed receipts). Comparing results of three types of nanocomposite particles prepared by the same CTS and MMA ratios, but varying in

their iron oxide contents (SAM1, SAM2, and SAM3 in Table 1), monomer conversation was enhanced with increasing the number of magnetic nanoparticles. When the weight ratio of CTS to MMA to MPS-coated γ-Fe_2O_3 nanoparticles was 15.2:18.2:4 (SAM 3), the monomer conversation and encapsulation efficiency were as high as 95% and 89%, respectively. The resultant nanocomposite particles contained 29.7% iron oxide as determined by the thermogravimetric analysis. When using higher chitosan to MMA ratio (SAM 4), the magnetic nanoparticle content of the nanocomposite particles could be up to 43.4%. these results suggest that it is possible to synthesize magnetic nanocomposite particles with the desired composition through altering ratios between chitosan, MMA monomer, and vinyl-coated γ-Fe_2O_3 nanoparticles.

Table 1

2.2 Chemical compositions of magnetic nanocomposite particles

The chemical structure of the γ-Fe_2O_3@PMMA/CTS nanocomposite particles (SAM2 sample) was identified using an FT-IR spectrometer. Figure S2 in the Supporting Information section shows spectra of pure PMMA, chitosan, γ-Fe_2O_3, and γ-Fe_2O_3@PMMA/CTS The spectrum of nanocomposite clearly shows characteristic peaks of chitosan (amine N-H and O-H stretching, 3300~3500 cm^{-1}; N-H bending, 1635 cm^{-1}; C-O stretching, 1150–1250 cm^{-1}), poly(methyl methacrylate) (C-H stretching, 2900-3100 cm^{-1}; ester carboxyl, 1731 cm^{-1}; C-H bending, 1485-1449 cm^{-1}; C-O stretching, 1150–1250 cm^{-1}) and iron oxide nanoparticles (γ-Fe_2O_3, 550-560 cm^{-1}) (Supporting Information **Table S2**). Thus the chemical composition of the nanocomposite particles was confirmed to consist of chitosan, PMMA, and iron oxide.

The crystallinity of iron oxide nanoparticles was examined by X-ray powder diffraction (XRD). Figure S3 (Supporting Information) compares the XRD profiles of γ-Fe_2O_3 nanoparticles, citrate-

coated γ-Fe_2O_3 nanoparticles, and γ-Fe_2O_3@ PMMA/CTS particles. All characteristic peaks of the iron oxide nanoparticles of the nanocomposite matched the crystallinity of standard γ-Fe_2O_3 nanoparticles (Card 39-1364 of the database of the International Center for Diffraction Data). These results indicate that surface modification and polymerization of the preformed γ-Fe_2O_3 nanoparticles did not affect the crystallinity of the γ-Fe_2O_3 nanoparticles.

2.3 Particle size and size distribution of the magnetic nanocomposite particles

Hydrodynamic diameters of four γ-Fe_2O_3@PMMA/CTS nanocomposite particles and their size distributions were determined by dynamic light scattering (DLS). Results shown in **Figure 1**a illustrate that using a high dosage of vinyl-coated γ-Fe_2O_3 magnetic nanoparticles (SAM 3) led to an increase in size and size distribution of the resultant nanocomposite particles. This effect might be attributed to the decrease in the solubility of chitosan in water after mixing it with vinyl-coated γ-Fe_2O_3 nanoparticles under ultrasonication before polymerization. The decrease in hydrophilicity of the chitosan resulted in increased size of the assembled domain during polymerization, which in turn led to the formation of bigger particles.[18] These results suggest that the particle size and magnetic nanoparticle content of the nanocomposite particles are easily tunable through varying the chitosan: MMA: vinyl-coated γ-Fe_2O_3 nanoparticles weight ratios.

Figure 1

2.4 Surface property of the magnetic nanocomposite particles

Colloidal stability and surface charge of the nanocomposite particles were determined by measuring the *zeta*-potential of the SAM 2 sample as a function of pH ranging from 2 to 11. A plot

of ζ-potential versus pH is shown in Figure 1b. The isoelectric point of the sample was at approximately pH 8, which was very close to the isoelectric point of the chitosan (pH = 8.5).[19] Moreover, ζ-potential values decreased from +45.7 mV to -15.2 mV with increasing solution pH. These results confirm the presence of the chitosan surface. The plot also indicates that the sample should be quite stable at pH values less than 7 since sufficient positive charge was present (> +20 mV). The positive charges at low pH values were due to the protonation of the amine groups of the chitosan, while the adsorption of hydroxyl ions led to the negative charges in an alkaline environment.

2.5 Morphology of magnetic nanocomposite particles

Figure 2a shows a SEM image of the γ-Fe_2O_3@PMMA/CTS nanocomposite particles (SAM2 sample). They appeared to have an irregular shape, and many of them had emerged together. Such particle aggregation might be induced by a strong magnetic attraction force between the particles during the drying process. To gain more insight into the real particle size, distribution, and aggregation in aqueous solution, nanoparticle tracking analysis using a NanoSight instrument was performed. Figure 2c shows a captured image of the nanocomposite particles in water from a video (Supporting document, Video). Individual particles, visualized as point scatters, were moving under Brownian motion. Few aggregates, which appeared brighter and moved more slowly due to increased hydrodynamic diameter, were observed. They were only transient aggregates induced by their magnetic attraction and could easily break up again. This visual validation confirms the very good dispersibility of the nanocomposite particles in water. The nanostructure of the nanocomposite particles (SAM2 sample) was also examined with TEM. Figure 2b reveals that

multiple magnetic nanoparticles were successfully entrapped and confined inside the PMMA core region of the nanocomposites.

Figure 2

2.6 Magnetic properties of the nanocomposite particles

The magnetic properties of citrate-coated γ-Fe_2O_3 nanoparticles and γ-Fe_2O_3@PMMA/CTS nanocomposites were determined by Vibrating Sample Magnetometry (VSM) analysis. **Figure 3**a shows that there were no hysteresis loops in either sample, indicating their superparamagnetic property, which is a favorable property for biomedical application of iron oxide-based nanocomposites. In addition, saturation magnetization (M_s) of citrate-coated γ-Fe_2O_3 nanoparticles and γ-Fe_2O_3@PMMA/CTS nanocomposites (SAM 2) were 61.1 and 11.6 emu per gram of particles, respectively. After deducting the weight of polymers in the nanocomposite, saturation magnetization of the embedded and aggregated γ-Fe_2O_3 nanoparticles was calculated as 87.9 emu per gram of maghemite, a value which is higher than that of the citrate-coated γ-Fe_2O_3 nanoparticles and the bulk γ-Fe_2O_3 (76 emu/g Fe).[20] Therefore, encapsulation of γ-Fe_2O_3 nanoparticles within the polymer matrix can improve the magnetic property of the nanocomposite particles for enhanced MR imaging.[21,22] To further evaluate the magnetic responsiveness of the nanocomposite particles in an aqueous solution, variation in particle concentration in water before and after exposure to a magnetic field was monitored by the nanoparticle tracking analysis. Figure 3b shows that the number of particles detected in the dispersion started to decrease after a permanent magnet was placed next to the sample cell of the instrument. Consequently, almost all the particles were attracted to the magnet side within 15 min, and the number of particles that

remained in the solution approached zero. These results indicate that the nanocomposite particles were highly susceptible to the magnetic field even in the aqueous system.

Figure 3

3. Property studies for MRI contrast agent

3.1 Stability of the magnetic nanocomposite particles in biological medium

Before the MR test, the stability of the nanocomposite particles in two biological media was evaluated by the DLS. Size variations of the γ-Fe_2O_3@PMMA/CTS nanocomposite particles (SAM2 sample) in both cell culture media, Dulbecco's modified Eagle's medium, (DMEM), and phosphate buffer saline (PBS), were monitored for up to 144 h. Results shown in **Figure 4**a suggest that the nanocomposite particles were very stable in DMEM, but slightly less stable in the PBS solution as reflected by the graduate increase in particle size with time.

Figure 4

3.2. Cytotoxicity study of the magnetic nanocomposite particles

The cytotoxicity of γ-Fe_2O_3@PMMA/CTS was evaluated in L929 mouse fibroblasts (normal cells) and HeLa cells (cervical cancer cells) by 3-(4,5-dimethylthiazol-2-y1)-2,5-diphenyltetrazolium bromide (MTT) assay. Results shown in Figure 4b illustrate that viabilities of both cell types were higher than 90% after treatment with γ-Fe_2O_3@PMMA/CTS nanocomposites for 24 h. These results suggest that the magnetic nanocomposite particles were biocompatible with the normal cells as well as the cancer cells. The low cytotoxicity of the γ-Fe_2O_3@PMMA/CTS particles demonstrates that they are safe and suitable for *in vivo* imaging purposes.[23]

3.3. In vitro and in vivo MRI Studies

To evaluate the MR imaging performance of γ-Fe_2O_3@PMMA/CTS nanocomposite particles, an *in vitro* MRI test was conducted using a clinical MRI instrument. **Figure 5** compares the T_2-weighted MR images of citrate-coated γ-Fe_2O_3 nanoparticles and γ-Fe_2O_3@PMMA/CTS nanocomposite particles as a function of iron oxide concentration. Figure 5a shows that the sample tubes containing γ-Fe_2O_3@PMMA/CTS nanocomposite particles have darker signals than those samples containing citrate-coated γ-Fe_2O_3 nanoparticles under the same iron oxide concentration. These results suggest that the nanocomposite particles may become excellent MR imaging contrast agents. To further verify this capability, the transverse relaxivity (r_2) values were calculated based on the T_2-weighted contrast of the MR imaging. Results shown in 5b indicate that the transverse relaxivity of γ-Fe_2O_3@PMMA/CTS nanocomposite particles was as high as 364 mM_{Fe}^{-1} s^{-1}, which is 2.4 times higher than that of the individually dispersed citrate-coated γ-Fe_2O_3 nanoparticles (r_2=152 $mM_{Fe}^{-1}s^{-1}$). This significant enhancement in r_2 values may be attributed to the aggregation and confinement of magnetic nanoparticles in the PMMA core as mentioned before. In fact, the r_2 value of 364 mM_{Fe}^{-1} s^{-1} is two to three times higher than that of some approved clinical T_2-type MRI contrast agents such as Feridex (r_2=98.3 $mM_{Fe}^{-1}s^{-1}$, AMAG Pharma) and Resovist (r_2=151 $mM_{Fe}^{-1}s^{-1}$, Bayer Healthcare).[24]

It was interesting to note that even though the aggregated magnetic nanoparticles were embedded in a water-impermeable hydrophobic core, the nanocomposite particle still possessed strong relaxivity. This effect may be attributed to the fact that the relaxation process of the superparamagnetic nanoparticle is mainly governed by the outer-sphere mechanism. The inner-sphere has minor or even negligible contribution.[25] Therefore, it is not necessary to have water

protons contracting the surface of the superparamagnetic nanoparticles. When the nanocomposite particles are placed in a magnetic field, they can produce strong magnetic perturbations because their magnetic moment is much greater than that of gadolinium chelates.[26] This magnetic perturbation could cause inhomogeneity of the local magnetic field, thus accelerating the diffusion and dephasing rate of water protons in the vicinity, resulting in enhanced relaxivities.[20]

Figure 5

To assess the MR imaging capability of the γ-Fe_2O_3@PMMA/CTS nanocomposite particles, we further conducted an *in vivo* test using a breast tumor-bearing mouse model with tail vein injection of nanocomposite particles into the mouse body. **Figure 6**a illustrates that signals for liver tissue became darker and darker with increasing circulation time to up to 80 mins. Concurrently, signals for the tumor site were also darkened. These results indicate that the magnetic nanocomposite particles could be used as an MR contrast agent for both liver and tumor imaging. Similar to other reported iron oxide-based MR contrast agents, the injected nanocomposite particles could specifically and passively target the liver tissue and the tumor region through the reticuloendothelial system (RES) and the enhanced permeability and retention (EPR) effect.[27] Analysis of signal intensity indicated that T_2 signal intensity gradually decreased to 80% at the tumor site, while significantly reduced to 60% at the liver. The enhanced contrast effect was able to remain for up to 80 min, thus allowing more time to perform *in vivo* imaging (Figure 6b). Therefore, the γ-Fe_2O_3@PMMA/CTS nanocomposite particles may be used as a long-time contrast agent in MR imaging diagnosis, especially for hepatic diseases.

Figure 6

4. Conclusion

We have developed a novel type of T_2-weighted MR contrast agent (γ-Fe_2O_3@PMMA/CTS), which consists of a biocompatible chitosan shell and a PMMA core embedded with aggregated γ-Fe_2O_3 nanoparticles. The nanocomposite particles have average sizes in the range of 300 to 400 nm with a narrow size distribution, as well as good stability in a physiochemical environment. Due to their high magnetization, superparamagnetic properties, and low cytotoxicity, we have evaluated their potential application as T_2-weighted MR contrast agent. The *in vitro* MR study suggests that the magnetic nanocomposite particle has excellent MR imaging performance with T_2 relaxivity up to 364 $mM_{Fe}^{-1}\cdot s^{-1}$, which is 2.4 times higher than that of the individually citrate-coated γ-Fe_2O_3 nanoparticles. The *in vivo* MR results further indicate that the magnetic nanocomposite particles could be used for both liver-specific and tumor MR imaging, Thus, the core-shell structured γ-Fe_2O_3@PMMA/CTS particle is a promising candidate for clinical application as a T_2-weighted MR contrast agent for MR imaging and imaging-guided cancer therapy, especially for liver-related diseases.

4. Experimental Section

4.1 Materials

Iron (II) chloride tetrahydrate ($FeCl_2\cdot 4H_2O$, Aldrich), anhydrous iron (III) chloride ($FeCl_3$, Fluka), ammonium hydroxide solution ($NH_3\cdot H_2O$, 25 wt.%, Aldrich), nitric acid solution (HNO_3, 68 wt.%, VWR) and trisodium citrate dihydrate ($C_6H_5O_7Na_3\cdot 2H_2O$, SAFC) were used as received. Tetraethyl orthosilicate [$Si(OC_2H_5)_4$], (International Laboratory USA), 3-(trimethoxysilyl)propyl methacrylate (MPS, Aldrich), methanol (CH_3OH, Lab-Scan) and ethanol (C_2H_5OH, VWR) were

used without purification. Methyl methacrylate (MMA, Aldrich) was purified by washing three times with a sodium hydroxide solution (10 wt.%), followed by washing with deionized water until the pH of the water layer dropped to 7. The monomer was then distilled for further purification. Chitosan of medium molecular weight (74% deacetylation) and glacial acetic acid ($C_2H_4O_2$, 99 wt.%) were purchased from Sigma-Aldrich. Milli-Q water was used as the dispersion medium. Dulbecco's modified Eagle's medium (DMEM, high glucose), fetal bovine serum (FBS, E.U.-approved, South America origin), Penicillin/Streptomycin (P/S, 10,000 U/mL), and (3-(4,5-dimethylthiazol-2-yl)-2,5-diphenyltetrazolium bromide) (MTT) were purchased from ThermoFisher Scientific.

4.2 Synthesis of γ-Fe_2O_3@PMMA/CTS nanocomposite particles

Vinyl-coated γ-Fe_2O_3 nanoparticles (MPS-Fe_2O_3) were synthesized according to our previously developed method.[10] The as-prepared vinyl-coated γ-Fe_2O_3 nanoparticles were purified by dialysis and then dispersed in ethanol for subsequent use. The γ-Fe_2O_3@PMMA/CTS nanocomposite particles were prepared according to the following procedure: For a total of 50 g of solution, chitosan powder (0.5 g) was dissolved in an acetic acid solution (0.6 *V*/*V* %, 44 mL). The preformed MPS-Fe_2O_3 nanoparticle dispersion (4.20 wt.% in ethanol) was charged dropwise to the chitosan solution and mixed with a homogenizer (Sonics VC130PB, output wattage = 6 W). After homogenization for 30 min, the dispersion was transferred to a water-jacketed flask equipped with a magnetic stirrer, a thermometer, a condenser and a nitrogen inlet. The dispersion was purged with nitrogen for at least 30 min at 80 °C. Purified MMA and H_2O_2 (final concentration was 0.1 mM) were added to the mixture, and stirred at 80 °C for 2 h under a nitrogen atmosphere. Dosages of MPS-Fe_2O_3 nanoparticles and MMA are shown in the Supporting Document (Table S1). After the reaction, the mixture was cooled down in an ice bath to terminate the polymerization, and

filtered to remove any precipitates. The MMA conversion was determined gravimetrically. The dispersion was purified by successive cycles of centrifugation (15000 rpm, 2h), decantation and re-dispersion until the conductivity of supernatant was closed to that of the Milli-Q water used. The purified nanocomposite particles were passed through a MACS® LS magnetic column with a QuadroMACS™ Separator to separate those particles containing no or little magnetic nanoparticles from the desired γ-Fe_2O_3@PMMA/CTS nanocomposite particles. The γ-Fe_2O_3@PMMA/CTS particles entrapped in the column were released by acetic acid solution (0.6 *V*/*V* %) in the absence of a magnetic field.

4.3 Characterization of Magnetic Nanocomposite Particles

1) Fourier Transformed Infrared (FT-IR) Spectral Studies: The IFTIR spectrum was recorded in the transmission mode on a Nicolet Avatar 360 FT-IR spectrophotometer. The dried samples were ground with KBr and the mixture was compressed into a pellet.

2) X-ray Powder Diffraction (XRD): The powder XRD pattern of γ-Fe_2O_3 nanoparticles was recorded by a BRUKER-AXS X-ray diffractometer (Bruker, Germany) with Cu target (40 KV, 40 mA) from 10 to 80º. Samples were dried under vacuum at room temperature overnight and then ground into fine powders before the measurement.

3) Particle Size and zeta-Potential Measurements: The hydrodynamic diameter and *zeta*-potential of citrate-coated γ-Fe_2O_3 nanoparticles and γ-Fe_2O_3@PMMA/CTS particles were determined by a Beckman Coulter Delsa™Nano C Particle Analyzer complemented with a Delsa™Nano Autotitrator. The photon correlation spectroscopy was obtained based on

electrophoretic dynamic light scattering from a two-laser diode light source at 658 nm wavelength at 30 mW. The scattering angle was set at 165°. Sample concentrations were between 200 and 400 mg/L. Hydrodynamic diameter, D_h, was calculated based on the Einstein Stokes equation $D_h = k_B T/3\pi\eta D$, where k_B is the Boltzmann constant, T is the temperature (K), η *i*s the viscosity of the dispersing medium, D is the diffusion coefficient obtained from the decay rate of the intensity correlation function of the scattered light (i.e., correlogrm), $G(\tau) = \int I(t)I(t+\tau)dt$. The results obtained were an average of triplicate measurement. *Zeta*-potential measurements were conducted in 1 mM NaCl aqueous solution at 25 ^{0}C.

4) Thermogravimetric Analysis (TGA): The composition of the MPS-coated γ-Fe_2O_3 nanoparticle was determined by TGA using a Netzch STA 449C Jupiter analyzer. The sample was dried at 50 °C at a nitrogen atmosphere for 5 mins and heated from 50 °C to 700 °C at a heating rate of 10 °C/min. The iron oxide content was calculated according to the following equation:

$$\text{MPS-}\gamma\text{-}Fe_2O_3 \text{ nanoparticles (\%)} = \frac{\text{sample weight at } 700^oC}{\text{sample weight at } 110^oC} \times 100\% \quad (1)$$

5) Scanning Electron Microscopy (SEM): The particle size, size distribution and morphologies of the particles were observed using a JEOL-JSM 6335 filed emission SEM at an accelerating voltage of 5 kV. The sample was prepared by spreading diluted sample dispersion onto a glass substrate, then allowing it to dry in a dust-free environment. The dried sample was coated with a thin layer of gold film with a depth of approximately 5 Å under vacuum.

6) Transmission Electron Microscopy (TEM): TEM images of samples were obtained using a transmission electron microscope (JEOL 100 CX) at an accelerating voltage of 100 kV. Samples were prepared by wetting carbon-coated grids with a small drop of dilute particle dispersion (100 mg/L). The grid was air-dried at room temperature before loading into the microscope.

7) Nanoparticle Tracking Analysis: Magnetic responsiveness and dynamic behavior of the dispersed samples were observed using a NanoSight Instrument. Diluted samples (20-100 mg/mL) were adjusted to pH 7 with sodium hydroxide solution, and injected into the sample cell of the instrument. Videos of the dynamic behavior of samples were recorded at room temperature. To evaluate the magnetic responsiveness of the nanocomposite particles in the aqueous system, a magnetic field was applied to the nanocomposite sample for approximately 10 mins by placing a permanent magnet next to the sample cell of the instrument. The recorded videos were then analyzed by the software of NanoSight Nanoparticle Tracking and Analysis (Version 2.3 Build 0034) with a detection threshold set to 20.

8) Vibrating Sample Magnetometer (VSM) Analysis: The saturation magnetization was determined using a VSM (PPMS Model 6000 Quantum Design, San Diego, USA). The magnetization measurements were conducted at room temperature under an external magnetic field H ranging from 0 to ±10,000 Oe.

9) Cell Culture: HeLa cells and L929 (mouse fibroblast) cells were cultured in a high glucose Dulbecco's modified Eagle's medium (DMEM), supplemented with 10% (*V*/*V*) fetal bovine serum

(FBS), 1% (*V*/*V*) penicillin/streptomycin (P/S) at 37 °C in a humidified atmosphere containing 5% CO_2.

10) In Vitro Cell Viability/cytotoxicity: The cytotoxicity of the γ-Fe_2O_3@PMMA/CTS particles was evaluated by the 3-(4,5-dimethylthiazol-2-yl)-2,5-diphenyl tetrazolium bromide (MTT) assay. L929 cells were seeded in 6-well plates with 1×10^5 cells per well, followed by treating the seeded cells with particles of different concentrations ranging from 5 to 200 μg/mL on a subsequent day. After incubation for 24 h with the particles and before the MTT assay, the cells were washed with PBS three times. MTT was dissolved in phenol red-free culture media and the MTT solution (1.2 mL, 0.83 mg/mL) was added to each well. After incubation for 4 h, acidified isopropanol (800 μL, 0.04 M HCl) was added to dissolve the insoluble formazan that had been formed. The number of viable cells in each well was determined by measuring the absorbance at 570 nm wavelength with a reference wavelength at 655 nm using a Microplate Reader (Bio-Rad Microplate Reader 680). The relative cell viability was calculated by comparing the absorbance of each group with that of the untreated cells. The results were the means of 3 replicates of each treatment. The cytotoxicity of the γ-Fe_2O_3@PMMA/CTS particles was also evaluated by MTT assay in HeLa cells using the same method as in the L929 cells.

11) In vitro MR Test: An in vitro MR test was performed to calculate the transverse relaxivity, r_2, of the γ-Fe_2O_3@PMMA/CTS nanocomposites. The MR imaging test was carried out in collaboration with Shanghai Cancer Hospital, which provided a 3.0 T MRI instrument (GE Signa HDx 3.0T, regulated by the regional ethic committee for animal experiments). To determine the transverse relaxivity (r_2) value, iron concentrations in the γ-Fe_2O_3@PMMA/CTS nanocomposite

particles were determined by inductively coupled plasma-atomic emission spectroscopy (ICP-AES) after dissolving the nanocomposites in a mixture solution of $HNO_3/HClO_4$ at 150 ºC. The T2-weighted MR images of samples at different iron concentrations were obtained by using a T2-weighted Fast-recovery fast spin-echo (FR-FSE) sequence with 2,000 ms repetition time (TR) and 110 ms echo time (TE). For T2 relaxivity measurement, the T2 relaxation time was performed with the following parameters: TR = 4000 ms, TE= 13, 26, 39, 52 ms. Relaxivity values of r2 were calculated through the curve fitting of 1/T2 relaxation time (s^{-1}) versus the Fe concentration (mM)

12) In Vivo MR Test: An *in vivo* MR test was executed on a naked mouse with a breast tumor. The naked mouse was tranquilized by Lidocaine (0.1 mL) through injection. After a pre-administration MR imaging scan, γ-Fe_2O_3@PMMA/CTS dispersion (0.2 mL, 1000 ppm) was injected into the naked mouse via the caudal vein. The final concentration of particles in the body was 10 mg/kg. The mouse was then taken for the MRI test which was performed using a 3.0 T clinical MRI instrument (GE Signa HDx 3.0 T). A fast spin-echo sequence (TR/TE = 4120/100 ms (T2), flip-angle = 90°, echo length = 10, field of view = 16 cm, slice thickness = 2 mm, matrix = 512 × 512 were used. Signal intensities (SIs) were measured in defined regions of interest (ROI), which were in comparable locations within tumor sites. Changes in relative signal values were calculated using SI measurement before (SIpre) and after (SIpost) injection of contrast agents, using the formula: [(SIpost − SIpre)/SIpre] × 100. The SIpost values were collected at 5, 20, and 80 min intervals.

Acknowledgment

This work was supported by the Hong Kong Ph.D. Fellowship Scheme (HKPF11-07529) of the Research Grants Council, Hong Kong Scholars Program (2013), China Postdoctoral Science Foundation (2014M560305), NSFC/RGC Joint Research Scheme (N_PolyU533/14), and PolyU Lo Ka Chung Centre for Natural Anti-Cancer Drug Development.

Received: ((will be filled in by the editorial staff))
Revised: ((will be filled in by the editorial staff))
Published online: ((will be filled in by the editorial staff))

References

[1] D. E. Lee, H. Koo, I. C. Sun, J. H. Ryu, K. Kim, *Chem. Sov. Rev.* **2012**, *41*, 2656.

[2] G. P. Yan, L. Robinson, P. Hogg, *Radiography* **2007**, *13*, e5.

[3] D. Ling, T. Hyeon, *Small* **2013**, *9*, 1450.

[4] Y. W. Jun, Y. M. Huh, J. S. Choi, J. H. Lee, H. T. Song, S. Kim, S. Yoon, K. S. Kim, J. S. Shin, J. S. Suh, J. Cheon, *J. Am. Chem. Soc.* **2005**, *127*, 5732.

[5] Z. Zhou, X. Zhu, D. Wu, Q. Chen, D. Huang, C. Sun, J. Xin, K. Ni, J. Gao, *Chem. Mater.* **2015**, *27*, 3505.

[6] J. T. Jang, H. Nah, J. H. Lee, S. H. Moon, M. G. Kim, J. Cheon, *Angew. Chem.* **2009**, *121*, 1260; *Angew. Chem. Int. Ed.* **2009**, *48*, 1234.

[7] J. Li, Y. Hu, J. Yang, W. Sun, H. Cai, P. Wei, Y. Sun, G. Zhang, X. Shi, M. Shen, *J. Mater. Chem. B.* **2015**, *3*, 5720.

[8] Y. Hu, J. Li, J. Yang, P. Wei, Y. Luo, L. Ding, W. Sun, G. Zhang, X. Shi, M. Shen, *Biomater. Sci*. **2015**, *3*, 721.

[9] Z. Yu, C. Peng, Y. Luo, J. Zhu, C. Chen, M. Shen, X. Shi, *RSC Adv*. **2015**, *5*, 76700.

[10] S. Tong, S. Hou, Z. Zheng, J. Zhou, G. Bao, *Nano Lett.* **2010**. *10*, 4607.

[11] J. H. Lee, Y. W. Jun, S. I. Yeon, J. S. Shin, J. Cheon, *Angew. Chem.* **2006**, *118*, 8340; *Angew. Chem. Int. Ed.* **2006**, *45*, 8160.

[12] D. Niu, Z. Liu, Y. Li, X. Luo, J. Zhang, J. Gong, J. Shi, *Adv. Mater.* **2014**, *26*, 4947.

[13] K. M. Ho, P. Li, *Langmuir* **2008**, *24*, 1801.

[14] K. M. Ho, W. Y. Li, C. H. Lee, C. H. Yam, R. G. Gilbert, P. Li, *Polymer* **2010**, *51*, 3512.

[15] A. Grützkau, A. Radbruch, *Cytometry, Part A* **2010**, *77A*, 643.

[16] S. Hak, P. E. Goa, S. Stenmark, F. F. Bjerkholt, O. Haraldseth, *Magn. Reson. Med.* **2015**, *74*, 858.

[17] Q. L. Vuong, P. Gillis, Y. Gossuin, *J. Magn. Reson.* **2011**, *212*, 139.

[18] P. Li, J. Zhu, P. Sunintaboon, F. W. Harris, *Langmuir* **2002**, *18*, 8641.

[19] S. H. Baek, B. Kim, K. D. Suh, *Colloids Surf., A* **2008**, *316*, 292.

[20] N. Lee, T. Hyeon, *Chem. Soc. Rev.* **2012**, *41*, 2575.

[21] N. Sethulakshmi, V. Sooraj, U. S. Sajeev, S. S. Nair, T. N. Narayanan, L. K. Joy, P. A. Joy, P. M. Ajayan, M. R. Anantharaman, *Appl. Phys. Lett.* **2013**, *103*, 162414.

[22] P. Kucheryavy, J. He, V. T. John, P. Maharjan, L. Spinu, G. Z. Goloverda, V. L. Kolesnichenko, *Langmuir* **2013**, *29*, 710.

[23] S. Shukla, A. Jadaun, V. Arora, R. K. Sinha, N. Biyani, V. K. Jain, *Toxicol. Rep.* **2015**, *2*, 27.

[24] Y. X. J. Wang, *Quant. Imaging Med. Surg.* **2011**, *1*, 35.

[25] S. L. C. Pinho, G. A. Pereira, P. Voisin, J. Kassem, V. Bouchaud, L. Etienne, J. A. Peters, L. Carlos, S. Mornet, C. F. G. C. Geraldes, J. Rocha, M. H. Delville, *ACS Nano* **2010**, *4*, 5339.

[26] K. E. Kellar, D. K. Fujii, W. H. H. Gunther, K. Briley-Sæbø, A. Bjørnerud, M. Spiller, S. H. Koenig, *J. Magn. Reson. Imaging* **2000**, *11*, 488.

[27] H. B. Na, I. C. Song, T. Hyeon, *Adv. Mater.* **2009**, *21*, 2133.

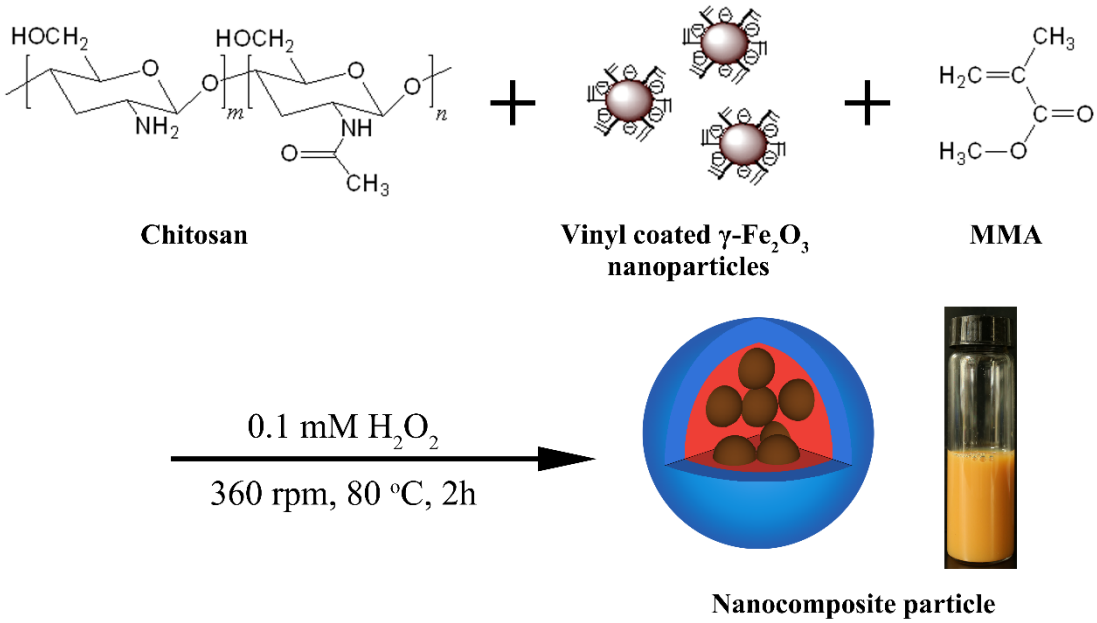

Scheme 1. Schematic diagram of the synthesis of γ-Fe_2O_3@PMMA/CTS nanocomposite particles

Table 1. Preparation of various samples of γ-Fe_2O_3@PMMA/CTS nanocomposite particles

Sample code	CTS : MMA : iron oxide (*w*/*w*) [a]	MMA Conversion [b] [%]	Encapsulation Efficiency [c] [%]	Composition of iron oxide [d] [%]	Mean diameter [nm]
SAM 1	15.2 : 18.2 : 1	69	66	26.7	341
SAM 2	15.2 : 18.2 : 2	79	85	29.4	395
SAM 3	15.2 : 18.2 : 4	95	89	29.7	607
SAM 4	15.2 : 6.1 : 1	76	83	42.4	368

[a)] Iron oxide means MPS-coated γ-Fe_2O_3 nanoparticles; [b)] Monomer conversions were determined gravimetrically according to the calculation shown in Table S1 in the Supporting information. [c)] Encapsulation efficiency was determined gravimetrically based on the amount of nanocomposite particles isolated from a crude product using a magnetic column with magnetic field gradients of 4 Tesla; [d)] Composition of nanocomposite particles was determined by a thermogravimetric analysis (Supporting information Figure S1).

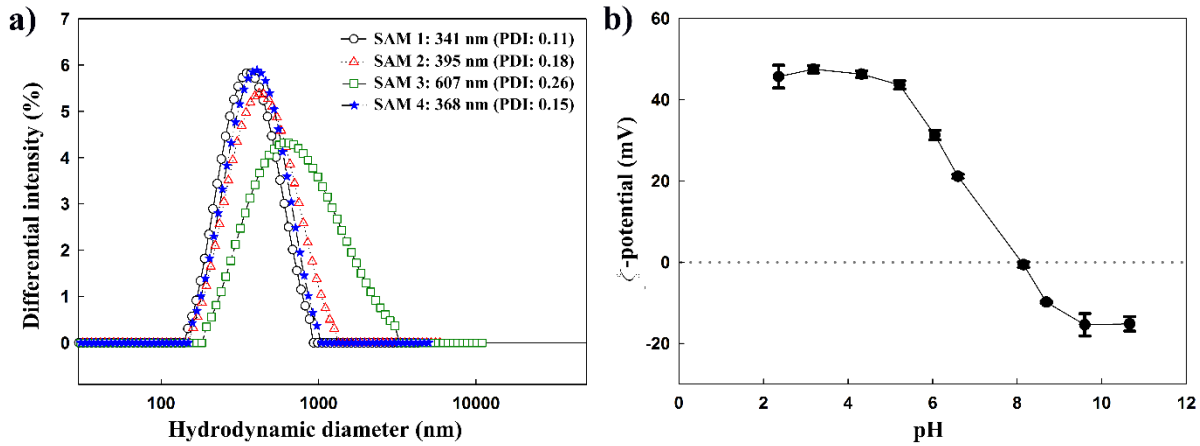

Figure 1. a) Size and size distribution of γ-Fe_2O_3@PMMA/CTS nanocomposite particles; b) *zeta*-Potential of γ-Fe_2O_3@PMMA/CTS nanocomposite particles (SAM 2) as a function of solution pHs.

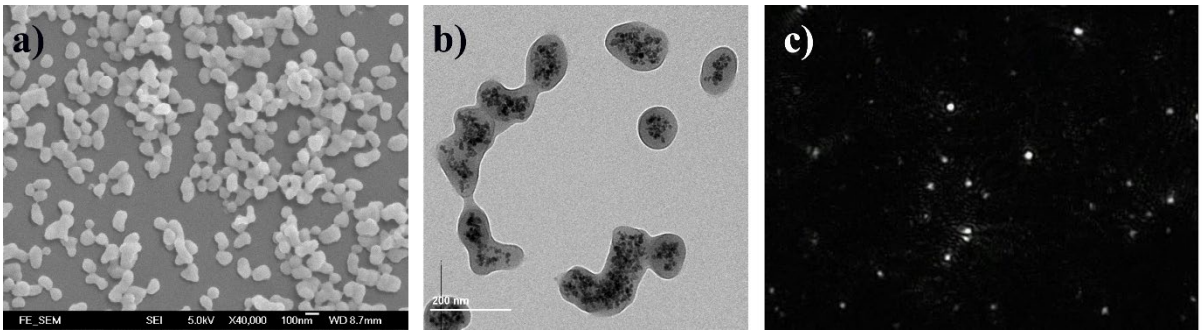

Figure 2. a) SEM image of the γ-Fe_2O_3@PMMA/CTS nanocomposites particles (SAM2 sample); (b) TEM image of the nanocomposite particles containing aggregated iron oxide nanoparticles in the hydrophobic core. (c) Captured video image of the nanocomposite particles using a NanoSight instrument.

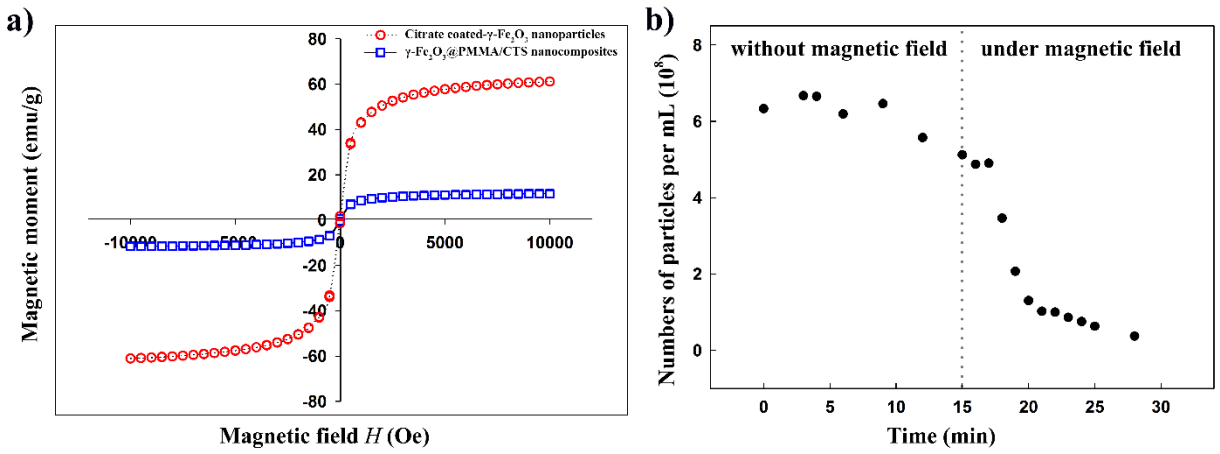

Figure 3. a) Hysteresis loop of citrate-coated γ-Fe_2O_3 nanoparticles (round circle) and γ-Fe_2O_3@PMMA/CTS nanocomposites (square). b) Changes in particle concentration in solution before and after applying a magnetic field.

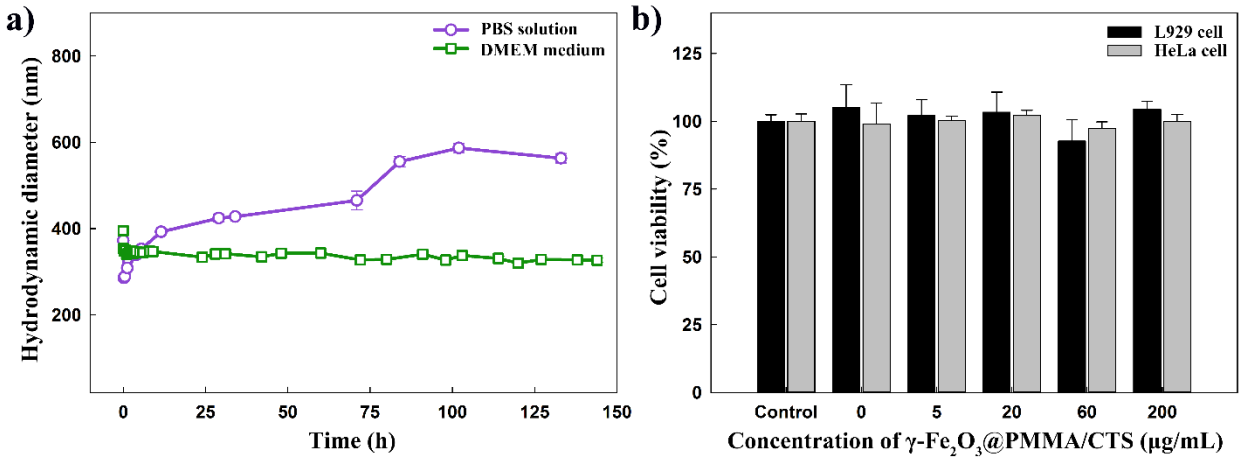

Figure 4. a) Stability of γ-Fe_2O_3@PMMA/CTS nanocomposite particles in PBS and DMEM mediums; b) Viabilities of HeLa and L929 cells cultured with γ-Fe_2O_3@PMMA/CTS nanocomposites (SAM2 sample) at different concentrations.

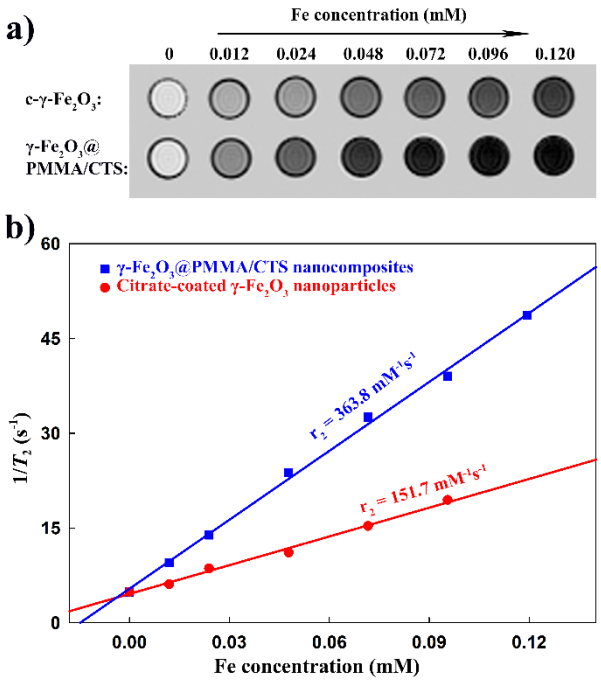

Figure 5. a) T_2-weighted MR images of citrate-coated γ-Fe_2O_3 nanoparticles and γ-Fe_2O_3@PMMA/CTS nanocomposites at different iron concentrations. b) Plots of the transverse relaxation rates (T_2^{-1}) against iron concentrations. The transverse relaxivities (r_2) were calculated based on the slopes of the stimulated regression lines.

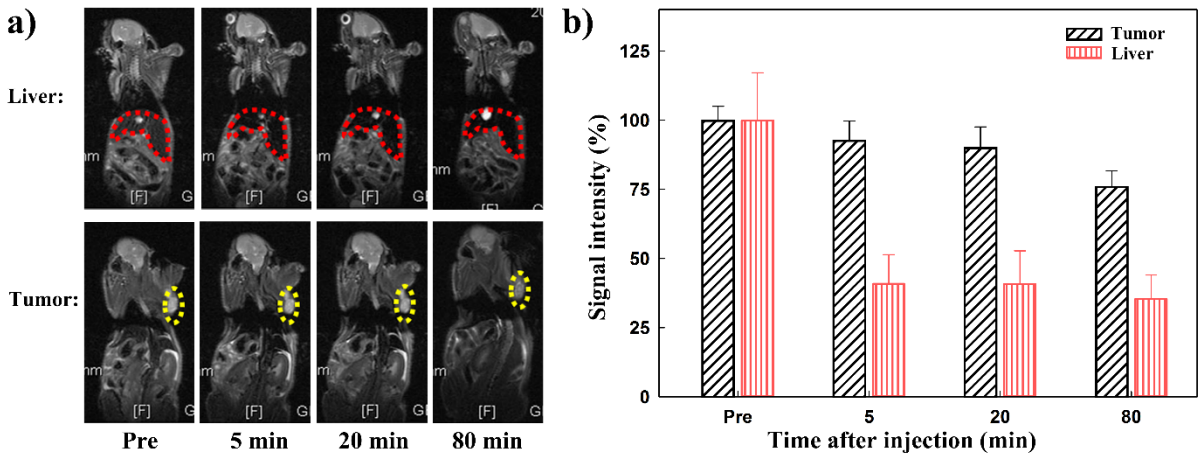

Figure 6. a) *In vivo* T_2-weighted MR images of a breast tumor-bearing mouse before and after administration of γ-Fe_2O_3@PMMA/CTS nanocomposite particles at different time points. (Red circle: normal liver tissue; yellow circle: tumor site) b) Signal intensities at different time points after administration of γ-Fe_2O_3@PMMA/CTS nanocomposite particles.

The table of contents entry should be 50–60 words long, and the first phrase should be bold. The entry should be written in the present tense and impersonal style. The text should be different from the abstract text.

Keyword: core-shell nanocomposite; magnetic nanoparticle; MRI contrast agent; T_2 relaxivity

L. Chen, D. Niu*, C. H. Lee, Y. Yao, K. Lui, K. M. Ho, Pei Li*

Title: Amphiphilic Core-Shell Nanocomposite Particles for Enhanced Magnetic Resonance Imaging

ToC figure

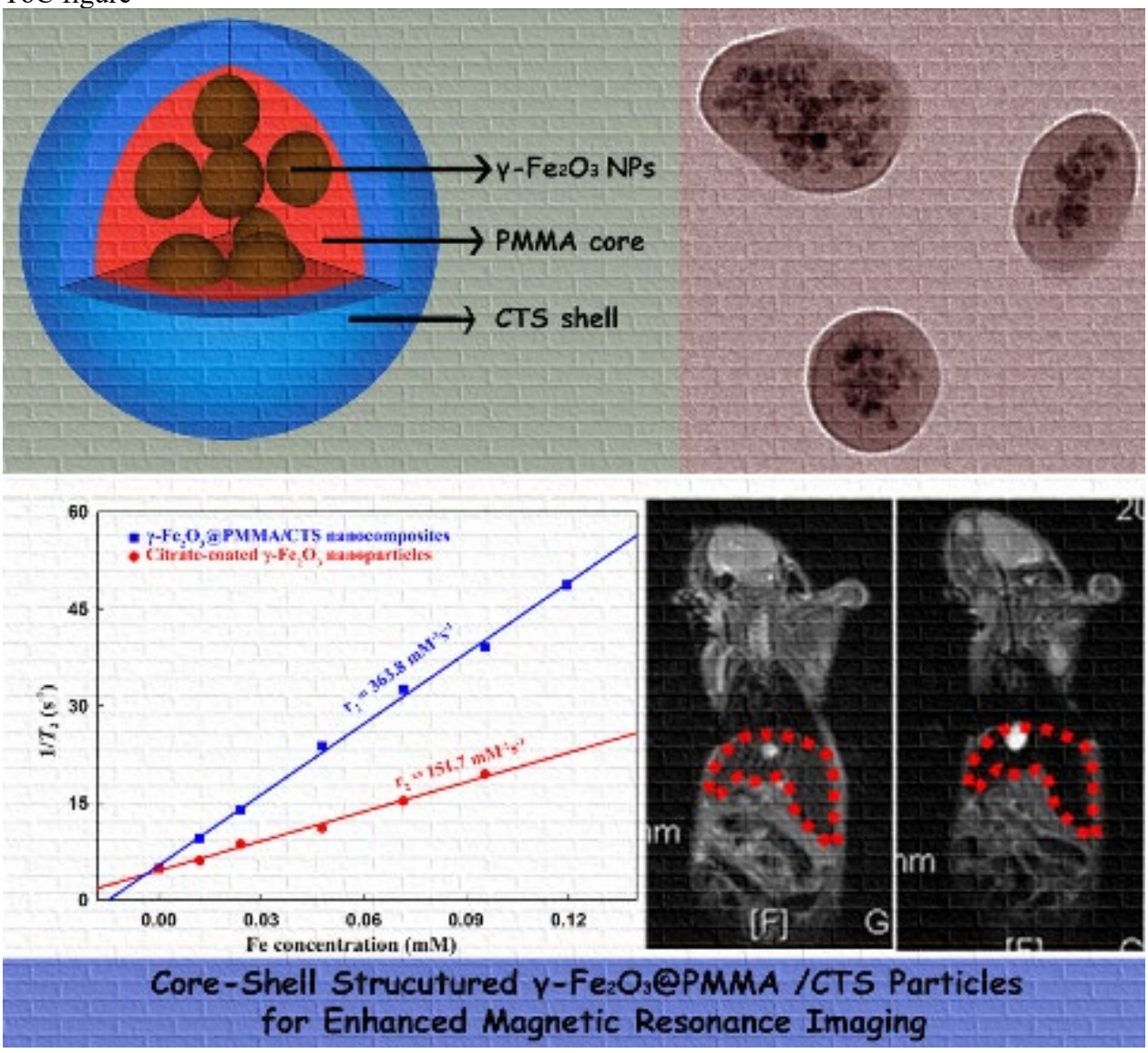

Supporting Information

Amphiphilic Core-Shell Nanocomposite Particles for Enhanced Magnetic Resonance Imaging

Lianghui Chen, Dechao Niu, Cheng Hao Lee, Yuan Yao, Ki Lui, Kin Man Ho, Pei Li**

Table S1. Receipts of the Synthesis of Four Magnetic Nanocomposite Particles

Sample	Chitosan [g]	MMA [g]	MPS coated γ-Fe_2O_3 nanoparticles [mg]	Weight ratio of CTS : MMA : γ-Fe_2O_3[a]	Monomer conversion [b] [%]
SAM 1	0.5	0.6	33	15.2 : 18.2 : 1	69
SAM 2	0.5	0.6	66	15.2 : 18.2 : 2	79
SAM 3	0.5	0.6	132	15.2 : 18.2 : 4	95
SAM 4	0.5	0.6	33	15.2 : 6.1 : 1	76

[a)] γ-Fe_2O_3 means MPS-coated γ-Fe_2O_3 nanoparticles. [b)] Monomer conversions were determined gravimetrically according to the following formula.

MMA conversion (%) = Weight of polymerized MMA / Weight of MMA monomer added x 100%

Weight of polymerized MMA = Solid content of the product – Weight of CTS – Weight of iron oxide

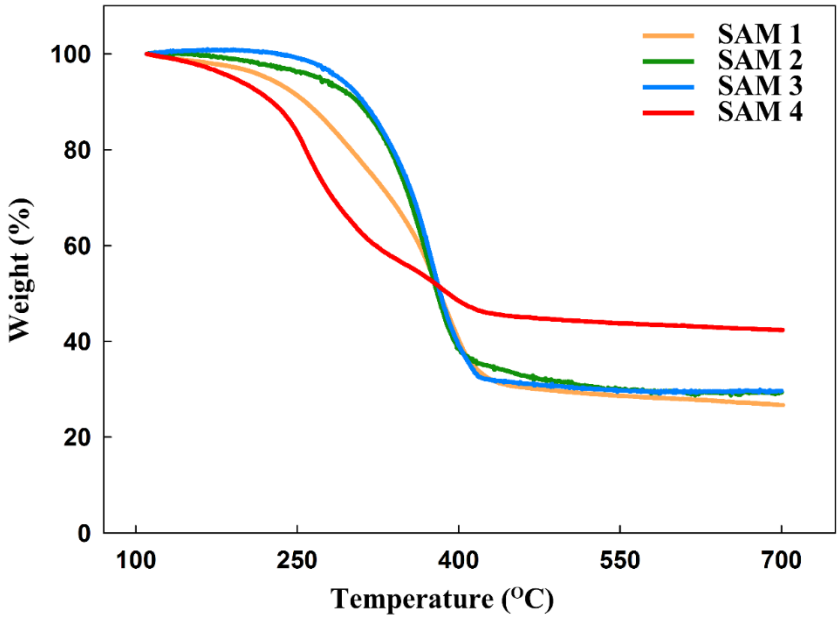

Figure S1. Contents of magnetic nanoparticles in various γ-Fe_2O_3@PMMA/CTS nanocomposite particles: SAM 1(orange line, 26.7%); SAM 2 (green line, 29.4%); SAM 3 (blue line, 29.7%); SAM 4 (red line, 42.4%).

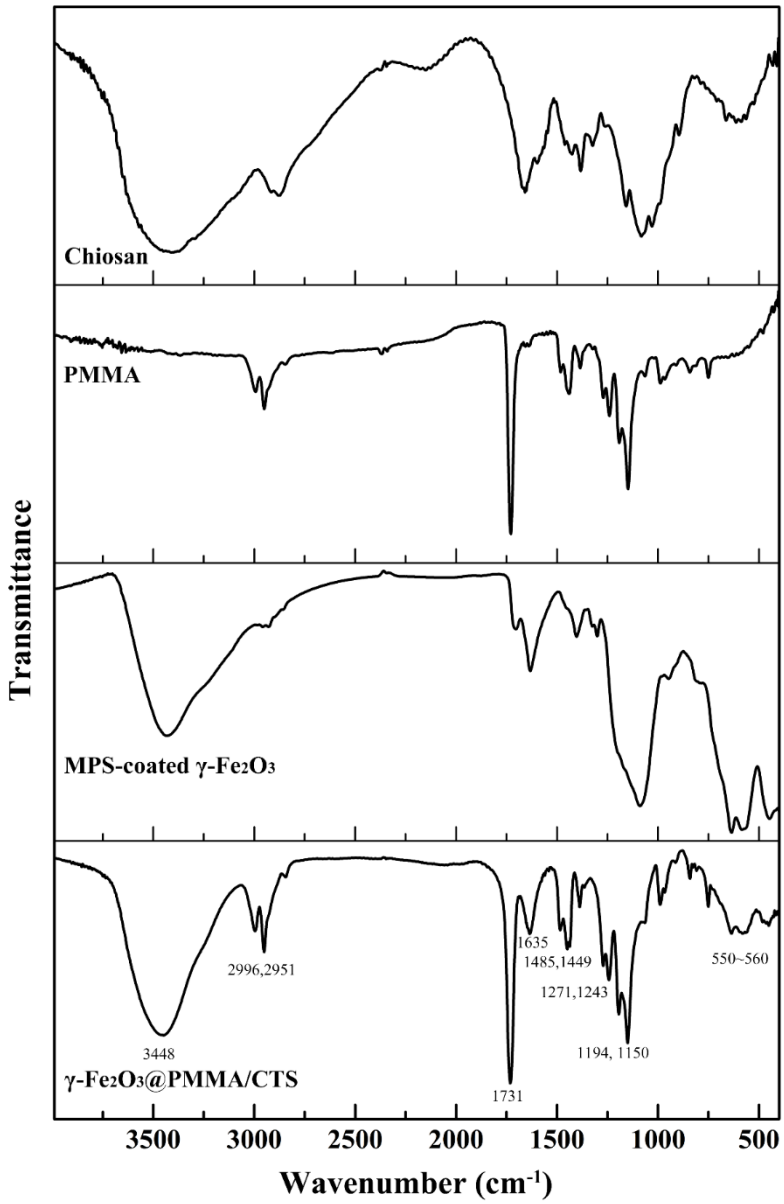

Figure S2. FT-IR spectrum of chitosan, PMMA (prepared by bulk polymerization), MPS-coated γ-Fe_2O_3 and γ-Fe_2O_3@PMMA/CTS nanocomposite particles prepared with weight ratio of CTS : MMA : MPS-coated γ-Fe_2O_3 NPs = 15.2 : 18.2 : 2 (SAM2 sample)

Table S2. Assignment of FT-IR characteristic peaks of γ-Fe_2O_3@PMMA/ CTS nanocomposite particles.

Wavenumber [cm^{-1}]	Assignment
3300~3500	Amine N-H stretching and/or O-H stretching
2900~3100	C-H stretching
~1730	Ester carboxyl group
~1635	N-H bending
1448~1490	C-H bending
1240~1275	C-O-C stretching of PMMA and C-O-H stretching of CTS
1150~1220	C-O–C stretching of PMMA and CTS
550~560	Fingerprint of γ-Fe_2O_3

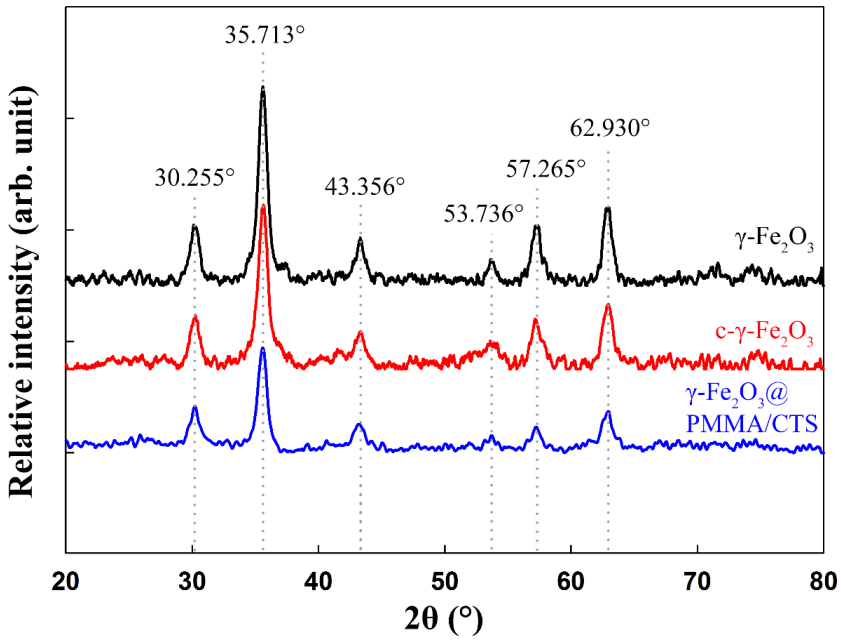

Figure S3. XRD profiles of γ-Fe_2O_3 nanoparticles (black line), citrate-coated γ-Fe_2O_3 nanoparticles (red line) and γ-Fe_2O_3@PMMA/CTS nanocomposite particles (blue line).

Nanosight video: